JET PROPULSION LABORATORY

INTEROFFICE MEMORANDUM

3411–96–336 ITP

November 25, 1996

TO: M. Colavita

FROM: J. W. Melody

SUBJECT: SIM Wavefront Tilt Disturbance Analysis and Angle Feedforward

SUMMARY:

This memorandum summarizes the SIM wavefront tilt disturbance analysis performed in IMOS. The analysis uses the SIM integrated model version 1.0. A brief summary of the model is given. The model is used to predict the differential wavefront tilt resulting from reaction wheel assembly (RWA) disturbances. By applying the analysis to various design cases, vibration control technologies are assessed for the science interferometer. Specifically, vibration isolation, structural quieting, and active optical control (*i.e.*, angle feedforward) are evaluated. The results indicate that only vibration isolation (with a break frequency $\leq$ 4 Hz) is necessary to meet the disturbance rejection requirements, in terms of differential wavefront tilt, for the science interferometer. Angle feedforward, which has limited effectiveness, is not needed. This result implies that the angle encoding requirements for the siderostat gimbals and fast steering mirrors can be relaxed.

Introduction

As part of the Space Interferometry Mission, an integrated modeling effort has been conceived in order to buy down SIM mission risk by answering questions related to instrument performance, requirements flow down, and design trades. These questions are addressed by performing various analyses on several integrated model versions. A phased model development incorporating these model versions is considered essential to the production of useful and timely results. The modeling plan is not described herein, but details are available from the author.

Using this nomenclature, this memo discusses the *question* of interferometer performance in the presence of mechanical disturbances by performing a disturbance *analysis* on the SIM integrated *model version* 1.0. In particular, the analysis considers the effect of reaction wheel disturbances on the stellar differential wavefront tilt for both guide and science interferometers. Initially, only reaction wheel disturbances are considered since they are expected to be by far the largest mechanical disturbances. Stellar differential wavefront tilt is predicted because it affects interferometer performance in terms of fringe visibility. Optical pathlength difference (OPD) also affects fringe visibility, but differential wavefront tilt is considered first in order to evaluate the necessity of angle feedforward. Angle feedforward, in turn, has implications for the siderostat gimbal and fast steering mirror (FSM) angle encoding requirements.

The analysis is used to assess the effectiveness of the layered vibration control technologies: vibration isolation, structural quieting, and active optical control (in this instance, angle feedforward) [1][2]. This is done by performing the analysis for four cases: 1) hard-mounted disturbance, no active optics, no structural quieting 2) isolated disturbances, no active optics, no structural quieting 3) isolation and quieting, with no active optics and 4) isolation, quieting, and angle feedforward. Furthermore, isolation pogo-mode break frequency is varied in order to make an initial estimate of isolator requirements. Finally, the effectiveness of angle feedforward separate from isolation and structural quieting is investigated.

Integrated Model Version 1.0 Description

Being the first in a series of models, the SIM integrated model version 1.0 is a relatively simple and nimble model that can be used quickly to gain general insights. The phased modeling plan allows for fidelity to be added to the subsequent models based on the knowledge gained from this model. In this spirit, model version 1.0 includes only a single baseline.

The modeling is performed in the Integrated Modeling of Optical Systems (IMOS) software package and uses the Controlled Optics Modeling Package (COMP) [3][4]. The SIM integrated model incorporates optics and structures models together much the same

as previous integrated models [5][6][7][8]. However, the controls model is dealt with differently because angle feedforward is being analyzed. A more detailed description of the integrated modeling process can be found in references [3][6][7].

Structural Model

The structural finite element geometry for model version 1.0 is shown in Figure 1. This geometry, based on that developed by L. Jandura, uses rigid body elements (shown as dashed lines) and beam elements (shown as solid lines) [9]. The circles in Figures 1 represent structural nodes. The finite element geometry includes two siderostat booms, one metrology boom, and one optics boom. The siderostat and metrology booms are modeled as flexible beams, while the optics boom is modeled as infinitely stiff (*i.e.*, with rigid body elements).

Each siderostat boom includes a model of a single siderostat bay. In Figure 1 these bays are at the ends of the booms. The position of each siderostat bay along the siderostat boom is parameterized such that any two of seven siderostat bay positions can be chosen. The possible siderostat positions, normalized by the baseline (*i.e.*, divided by 5 m), are [1, 0.868, 0.694, 0.116] for the positive x-axis boom and [-1.0, -0.918, -0.526] for the negative x-axis boom. These positions are numbered from the outside in, hence a particular baseline is specified as (p1,n2), where p refers to the positive x-axis boom, n refers to the negative boom, and (1,2) refer to the respective positions. For instance, in Figure 1 the baseline shown is (p1,n1). Each siderostat bay is modeled with several nodes rigidly connected together: a mass node containing the estimated lumped mass of the bay and optics nodes at the locations of the siderostat, beam compressor, and FSM optical elements.

The optics boom contains nodes for the RWA disturbance location, the switchyard mirrors, one set of passive and active delay lines, a single beam combiner, and when isolation is used, the hexapod isolator. The hexapod is not shown in Figure 1. The RWA disturbance location can be seen in Figure 2, which shows the bare-boom geometry with the isolator included. The isolator incorporates only the axial stiffness of the six isolator struts, in the appropriate hexapod geometry. The stiffness of the struts is parameterized according to the pogo-mode frequency. Aside from the isolator, all nodes of the optics boom are rigidly connected.

The metrology boom includes the lumped mass of the beam launcher truss at the end of the boom. The bending properties of the siderostat booms and the metrology boom were chosen so that each boom would have a fixed-free first bending mode of 5 Hz [9]. The lowest global flexible body mode of the structure is 7.85 Hz.

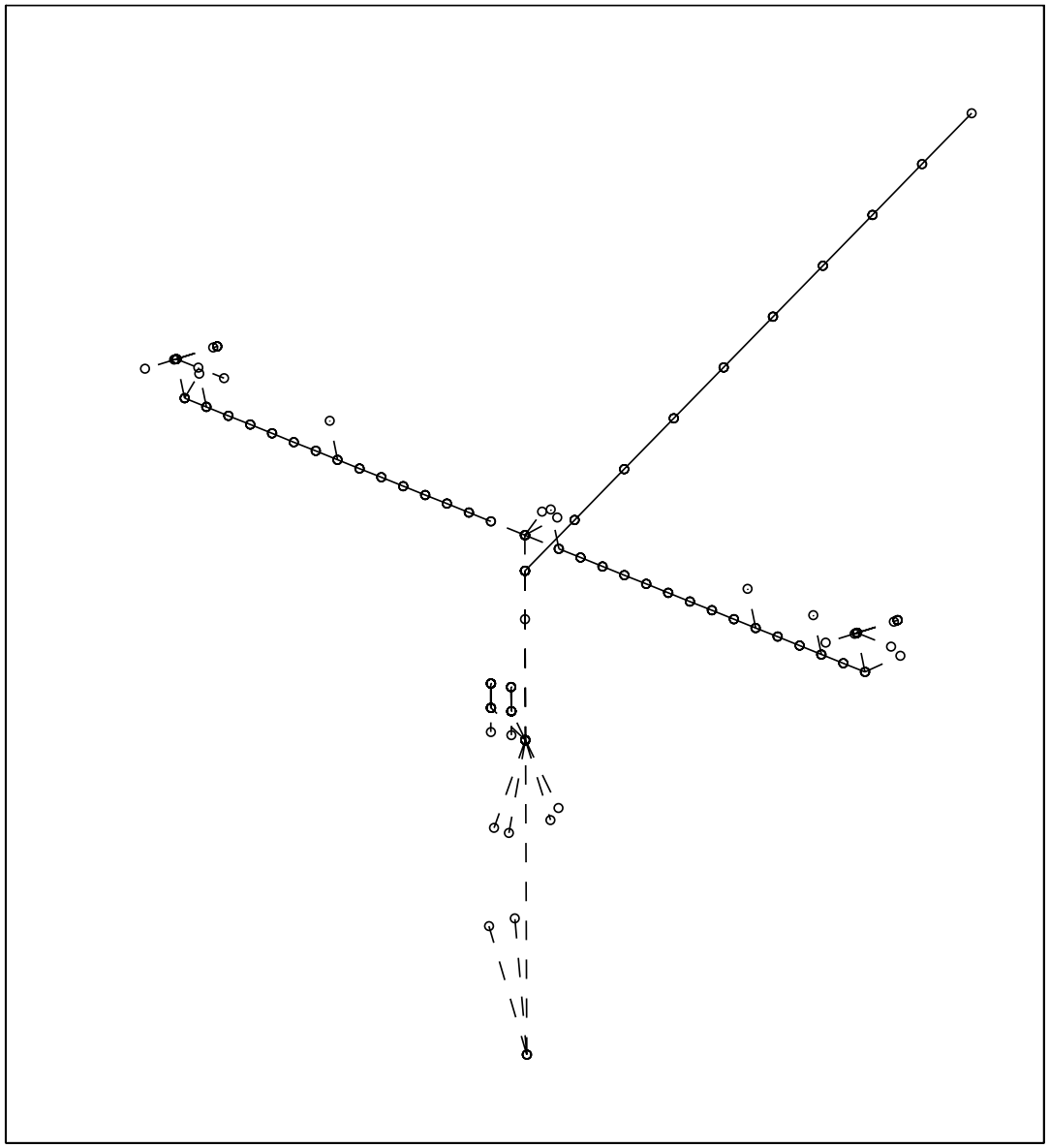

Figure 1: SIM model version 1.0 finite element geometry. Dashed lines are rigid body elements, solid lines are beams, and circles are nodes.

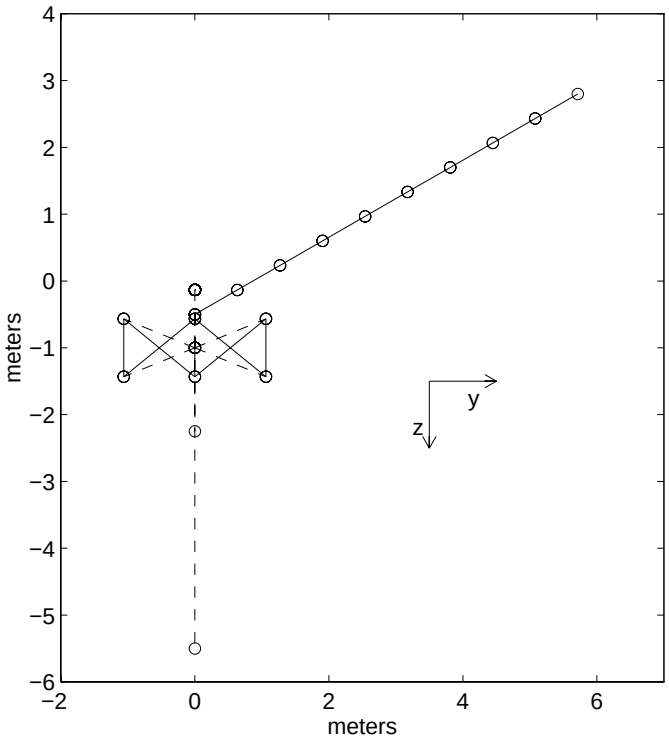

Figure 2: SIM model version 1.0 finite element geometry of the bare booms and hexapod isolator only: side view.

Optical Model

The SIM model version 1.0 includes optical models of a single stellar interferometer and its corresponding internal metrology system. Because the model includes only a single interferometer, no external metrology is modeled. As with the structural model, the optical model is parameterized according to siderostat location. A ray trace of the optical models plotted on top of the structural model is shown in Figures 3 and 4. Note that the internal metrology system is not used in the DWT disturbance analysis. The optical prescriptions are based on those created by E. Schmidtlin [10].

Model Integration

With the component models defined, they can be integrated into a single state-space model [3]. In the process of integration, modal truncation of the structural model is performed in order to reduce the computational burden of the analysis. The global modes are truncated according to their frequency, whereas all modes associated with the isolation are kept (when isolation is included). Global modes below 1 kHz (49 modes) are kept,

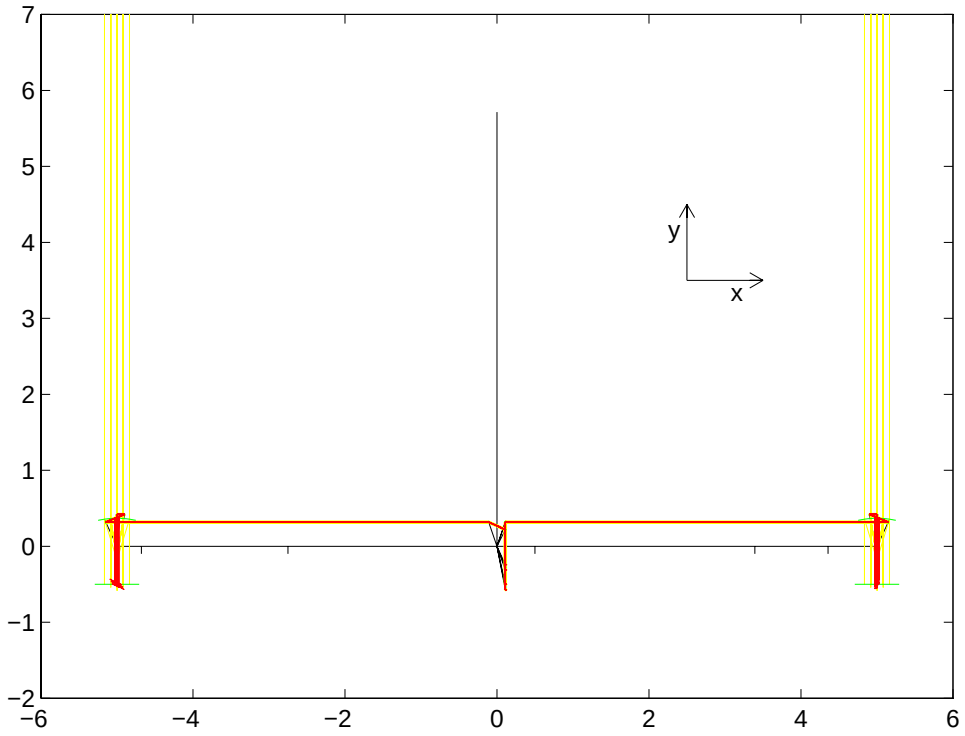

Figure 3: SIM model version 1.0 optical prescription: top view.

along with six isolator modes and six rigid body modes.

During integration, modal damping is assigned to the structural model. Modal damping has been measured on the MPI testbed as low as 0.1%. However, there is evidence to suggest that modal damping of similar structures may increase to 1% in a spaceborne environment [11][12]. Adhering to a policy of erring on the conservative side, a modal damping of 0.1% is used. Structural quieting is modeled by increasing the modal damping of targeted modes. The amount of damping obtained can be estimated from previous damper placement analysis and implementations [2][13]. Conversely, the damping can be parameterized, allowing generation of structural quieting requirements.

For this analysis, the integrated model provides a transfer-function description of the system from RWA disturbance input to stellar DWT output. The DWT output of the model are DWT about the two axes in the plane of the detector, $DWT_x(t)$ and $DWT_y(t)$. The quantity that affects the fringe visibility, however, is the magnitude of the vector sum of the DWT about the two detector axes, referred to as the total DWT:

$$DWT(t) = \sqrt{DWT_x^2(t) + DWT_y^2(t)} \tag{1}$$

Total DWT is used in the disturbance analysis.

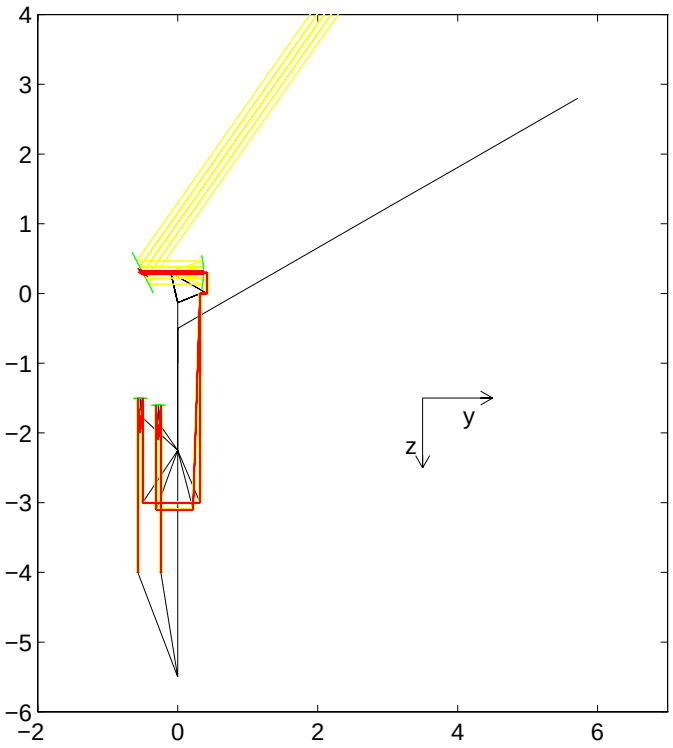

Figure 4: SIM model version 1.0 optical prescription: side view.

RWA Disturbance Analysis Description

Along with transfer functions, the disturbance analysis requires a spectral description of the RWA disturbances. For simplicity, only a single RWA is modeled. The other wheels are accounted for by assuming that the DWT resulting from all of the wheels are the same, hence the DWT requirement can be separated out for each wheel. This is a fairly valid assumption, as the model has shown that the disturbance analysis is roughly invariant with respect to wheel orientation (to within less than a factor of three). Furthermore, this analysis is over-bounding, since the worst-case orientation is used.

The RWA disturbance analysis is based on a disturbance model generated from testing of the Hubble Space Telescope flight units [14]. According to this model, the force and torque vibrations emanating from the RWA are sinusoidal harmonics of the wheel speed whose amplitudes are proportional to the wheel speed squared.

Since the RWA disturbances are dependent upon the wheel speed, a wheel speed must be given in order to perform a disturbance analysis. Unfortunately, the wheel speed during observations will vary as the spacecraft attitude control system reacts to external torques. The extent to which this variation occurs is dependent upon the characteristics of

the momentum management system and the external torques. Furthermore, if the wheels are biased at different speeds, momentum will be transferred between wheels during a slew. This results in a change of *separate* wheel speeds after a slew, even though the overall angular momentum remains unchanged by the slew. For these reasons, the wheel speeds can vary over a wide range. Therefore, the performance analysis must be parameterized by wheel speed.

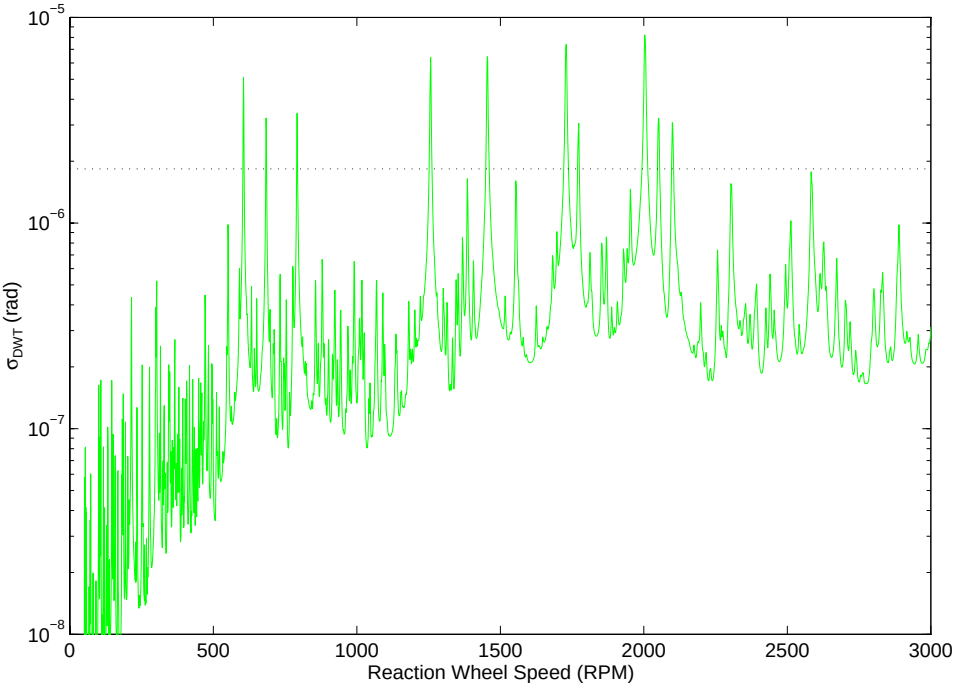

Figure 5: Total Stellar DWT for a hardmounted disturbance, no structural quieting, and no active optics: interferometer (p1,n1).

The disturbance analysis is described in great detail for optical pathlength difference in [15]. Essentially, for every wheel speed, autospectra of the wheel disturbances are generated, filtered through the disturbance transfer functions, and added together in order to obtain the autospectra of the two differential wavefront tilts, $DWT_x(t)$ and $DWT_y(t)$. These autospectra are then integrated to yield the respective variances. Finally, the variance of total DWT is obtained as the sum of the detector x- and y-axis variances.

The total DWT standard deviation, σ_{DWT}, is then plotted as a function of wheel speed. As an example, σ_{DWT} versus wheel speed for a hardmounted disturbance, no structural quieting, and no active optics (case 1 mentioned above) is shown in Figure 5.

The dashed line in Figure 5 represents the total DWT requirement *applied to one wheel*. The derivation of this requirement is given in [6], and is consistent with [16].

Given a stellar beam width of 3 cm at the detector, an instrument center wavelength of 550 nm, and a fringe visibility requirement for four wheels of 90% divided evenly between DWT and OPD, the requirement is 1.8 μrad.

Angle Feedforward

At its simplest, angle feedforward refers to taking the differential wavefront tilts from at least one guide interferometer and feeding them forward to the science interferometer. This is desirable since the science interferometer will often be observing objects so dim that the photon noise of the wavefront tilt measurement limits the control bandwidth to less than one Hertz. In other words, the science interferometer wavefront tilt control system cannot provide disturbance rejection in the expected mechanical-disturbance frequency regime. Angle feedforward seeks to provide an estimate of the science interferometer wavefront tilts from the guide interferometer wavefront tilt commands. This is analogous to the pathlength feedforward save for two significant differences: 1) whereas the OPD is largely effected by rigid-body motion common to both interferometers, DWT is almost primarily a result of flexible-body motion different for each interferometer and 2) the angle feedforward does not have the benefit of either an external or internal metrology system to measure the effects of motion of the optical elements as does the pathlength feedforward.

Since the SIM model version 1.0 has only one interferometer, the angle feedforward cannot be modeled directly. Instead, the guide and science interferometers are modeled separately by exploiting the siderostat location parameterization. Each model results in RWA disturbance to wavefront tilt transfer functions. These transfer functions are then manipulated with block-diagram techniques in order to obtain the effective disturbance transfer functions of the science interferometer with angle feedforward. These effective disturbance transfer functions are then used in the RWA disturbance analysis described above.

The block diagram of angle feedforward is shown in Figure 6, where G is the plant transfer function matrix, K is the controller transfer function matrix, D is the disturbance transfer function matrix, T_{ff} is a transform matrix discussed below, and the subscripts g and s refer to guide and science interferometers, respectively. For both interferometers, G has as its input the four FSM commands (two interferometer arms, two axes each) with output of four wavefront tilts (two arms, two detector axes), hence it is a four-by-four transfer function matrix. Similarly, K is four-by-four. Generally, both G and K are diagonally dominant and can be approximated as four separate single-input, single-output (SISO) transfer functions. The disturbance transfer functions, D, have four wavefront tilt output and six input for the RWA disturbance forces and torques.

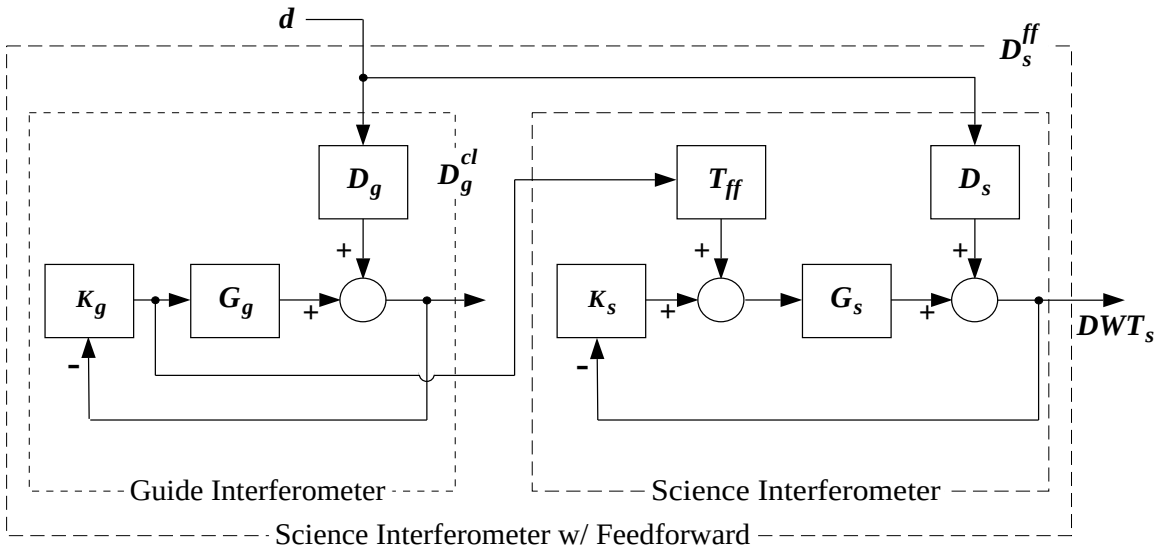

Figure 6: Angle feedforward block diagram description: d ($\epsilon\ \mathcal{R}^6$) is disturbance input and DWT_s ($\epsilon\ \mathcal{R}^4$) is differential wavefront tilt output.

The closed-loop disturbance transfer function of the guide interferometer, $D_g^{cl}(s)$, is given by:

$$D_g^{cl}(s) = \left[I + G_g(s)K_g(s)\right]^{-1} D_g(s) \tag{2}$$

Since the guide interferometer is observing a bright star, the wavefront tilt control system will generally have a bandwidth of 100 Hz or more, and the sensitivity transfer function, $S_g(s) = \left[I + G_g(s)K_g(s)\right]^{-1}$, will attenuate disturbances roughly up to this bandwidth. As mentioned above, the science interferometer will have a bandwidth low enough that the feedback can be ignored in the frequency regime of expected RWA disturbances. In other words, $\bar{\sigma}\left[G_s(j\omega)K_s(j\omega)\right] \approx 0$ where $\bar{\sigma}\left[\cdot\right]$ denotes the largest singular value of the argument [17]. Hence, without angle feed forward the closed-loop disturbance transfer function of the science interferometer, $D_s^{cl}(s)$, is given by:

$$\begin{aligned} D_s^{cl}(s) &= \left[I + G_s(s)K_s(s)\right]^{-1} D_s(s) \\ D_s^{cl}(s) &\approx D_s(s) \end{aligned} \tag{3}$$

The resulting angle feedforward disturbance transfer function of the science interfer-

ometer (using the approximation in Eq. 3) is:

$$\begin{aligned} D_s^{ff}(s) &= S_s(s)\left[D_s(s) - G_s(s)T_{ff}(s)K_g(s)S_g(s)D_g(s)\right] \\ D_s^{ff}(s) &\approx D_s(s) - G_s(s)T_{ff}(s)K_g(s)S_g(s)D_g(s) \end{aligned} \tag{4}$$

where $S_s(s) = [I + G_s(s)K_s(s)]^{-1}$ is the science interferometer sensitivity transfer function.

Since $\underline{\sigma}[G_g(\jmath\omega)K_g(\jmath\omega)] \gg 1$ up to the bandwidth of the guide interferometer, with $\underline{\sigma}[\cdot]$ specifying the smallest singular value, we can use the following approximation:

$$S_g(s) \approx K_g^{-1}(\jmath\omega)G_g^{-1}(\jmath\omega) \quad \text{for } \omega < \omega_n \tag{5}$$

where ω_n is the guide interferometer bandwidth.

Incorporating this approximation, Eq. 4 reduces to:

$$D_s^{ff}(\jmath\omega) \approx D_s(\jmath\omega) - G_s(\jmath\omega)T_{ff}(\jmath\omega)G_g^{-1}(\jmath\omega)D_g(\jmath\omega) \quad \text{for } \omega < \omega_n \tag{6}$$

If good estimates exist for $G_s(\jmath\omega)$ and $G_g(\jmath\omega)$ when $\omega < \omega_n$, then the effects of differing plant transfer functions can be accounted for with T_{ff}. This is plausible, since the plant transfer functions are typically constant out to several hundred Hertz [18]. Unfortunately, since the disturbance transfer functions have very rich modal content, no such estimate can be made for them.

Suppose that these estimates are available ($\hat{G}_g$ and $\hat{G}_s$). Then for $T_{ff} = \hat{G}_s^{-1}\hat{G}_g$, the angle feedforward disturbance transfer function is given by:

$$D_s^{ff}(s) \approx D_s(s) - D_g(s) \tag{7}$$

In other words, the angle feedforward will be effective within the bandwidth of the guide interferometer insofar as the two disturbance transfer functions are equal. This is consistent with intuition. Potential reasons for differences in D_s and D_g are differing siderostat locations and differing siderostat orientations. The former will always be true for the present SIM design, but can be minimized by judicious choices of baselines. The latter is true to the extent that the two interferometers view different stars. Unfortunately, the pathlength feedforward sets a minimum requirement on angular separation of the guide and science targets [19].

Disturbance Analysis Results

The disturbance analysis results were used to assess the effectiveness of vibration isolation, structural control, and angle feedforward by evaluating four cases: 1) hardmounted disturbance, no active optics, no structural quieting 2) isolated disturbances, no active

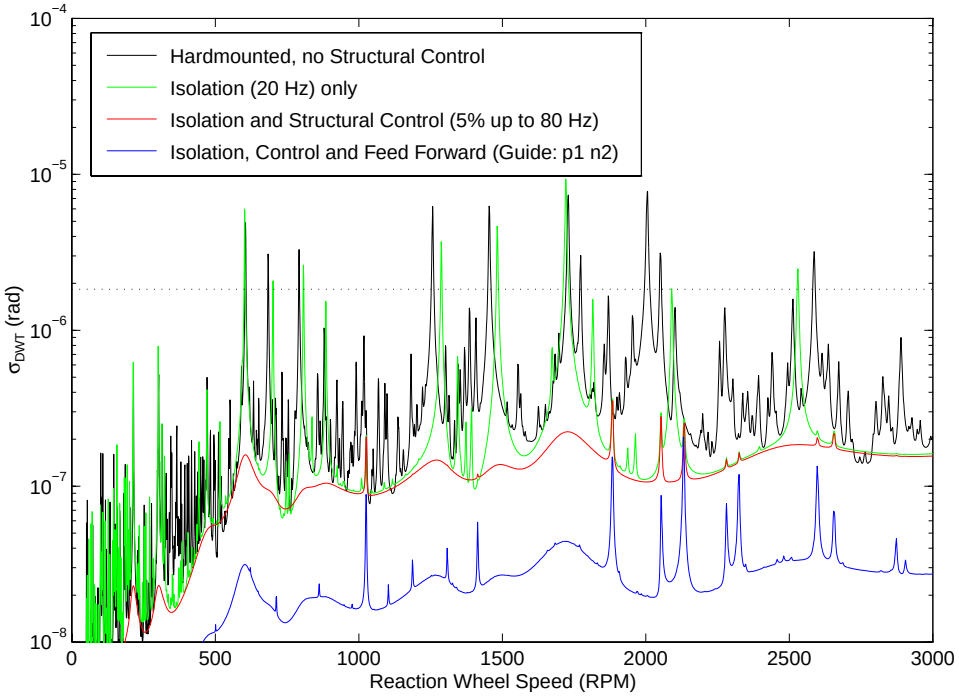

Figure 7: Stellar differential wavefront tilt disturbance analysis: guide interferometer (p1,n2), science interferometer (p2,n1).

optics, no structural quieting 3) isolation and quieting, with no active optics and 4) isolation, quieting, and angle feedforward. Each case used a science baseline of (p1,n2) and the angle feedforward assumed a guide baseline of (p2,n1). These baseline are as close to symmetric as possible, and hence, along with the assumption that both interferometers are viewing the same star, represent a best-case analysis of the angle feedforward. The isolator model used a pogo-mode break frequency of 20 Hz, consistent with existing hardware. Furthermore, a modal damping of 10% was used for the isolator modes, which corresponds to the use of active isolation. Structural quieting was modeled by assuming a 5% modal damping of flexible-body modes up to 80 Hz (17 modes).

The results for these four cases are shown in Figure 7. For these cases both isolation and structural control are needed to meet the requirement. Further evaluation of the data shows that the vibration isolation is sufficiently attenuating disturbances above roughly 80 Hz, but the structural quieting is needed for flexible-body modes up to 80 Hz. In fact, 80 Hz was chosen interactively to meet the DWT requirement. Angle feedforward, while effective in this case, was not necessary to meet the requirements.

Vibration Isolation Requirement

Because structural quieting will add cost and complexity, its use is undesirable. For this reason, the disturbance analysis was used to determine the requirements on the isolation pogo-mode break frequency if only isolation is used. This was done by performing the disturbance analysis on the isolation-only case (*i.e.*, no angle feedforward nor structural quieting) for different values of pogo-mode break frequency. In each analysis, the isolator modes are assumed to have modal damping of 10% as above. The worst-case science baseline for isolation, (p1,n1), was used.

Break Frequency (Hz)	$\max\{\sigma_{DWT} : RPM \epsilon [0, 3000]\}$ (μrad)
no isolation	8.2
20.0	9.9
6.0	5.0
4.6	2.3
requirement	*1.8*
3.5	1.2
2.0	0.4

Table 1: Maximum total DWT over wheel speed as a function of isolator pogo-mode break frequency.

The results of the isolation requirements analysis are tabulated in Table 1, where the maximum total DWT is listed as a function of the isolation break frequency. In order to meet the total DWT requirement, the isolator pogo-mode break frequency must be ≤ 4 Hz. Figure 8 plots σ_{DWT} for the hardmounted disturbance and several isolator designs.

It is important to remember that the isolator requirement of ≤ 4 Hz derives only from the total DWT requirement. A more stringent requirement may be derived from OPD, although based on previous interferometer disturbance analyses this is not expected to be the case [6]. Furthermore, isolation is effective only for targeted disturbances at discrete locations, whereas structural quieting and angle feedforward are effective for all disturbances, regardless of disturbance location. This analysis addresses RWA disturbances since they are expected to be the largest. Even so, there may be distributed disturbances, such as structural creak or atmospheric buffeting, that cannot be isolated and will have a more significant impact than the *isolated* RWA disturbances.

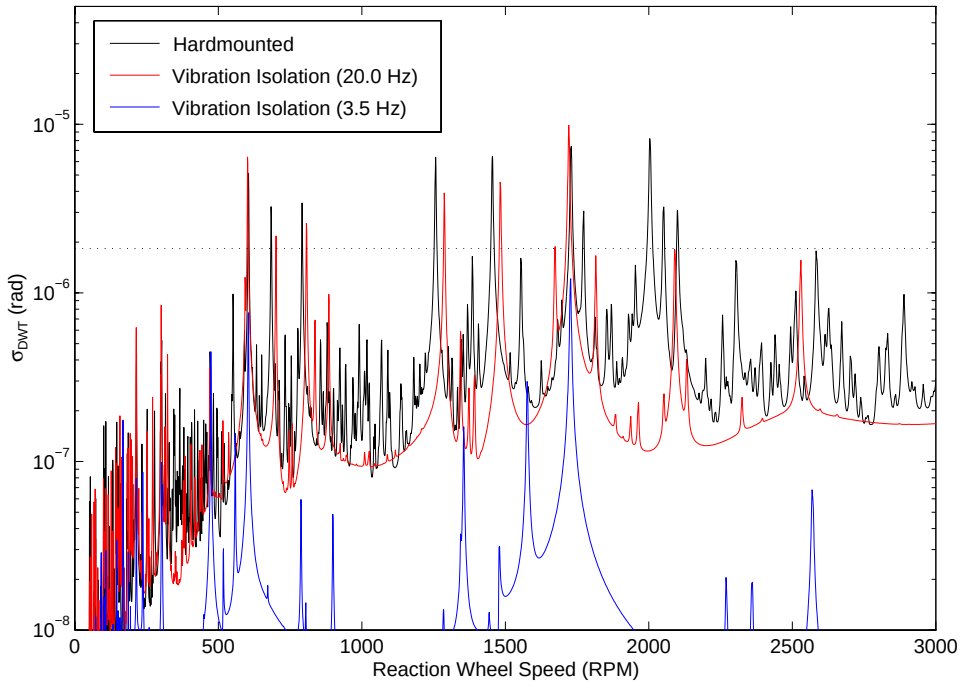

Figure 8: Stellar differential wavefront tilt disturbance analysis: isolation break frequency requirements for science interferometer (p1,n1).

Effectiveness of Angle Feedforward

Although isolation attenuates RWA disturbances sufficiently to meet the total DWT requirement, it is useful to investigate the effectiveness of angle feedforward should a new design or set of requirements deem it a necessary option. Figure 7 showed that angle feedforward could provide some improvement. However, this analysis used the best-case selection of siderostat locations, as well as assuming that both interferometers are viewing the same star. Both of these assumptions are revisited in this section.

Angle feedforward is assessed by considering combinations of the best-case and worst-case siderostat locations with the best-case and worst-case siderostat orientations. This is illustrated in Table 2, where the interferometer pairs (p1,n1) and (p2,n3) are the worst-case siderostat positions; (p1,n2) and (p2,n1) are the best-case positions; the worst-case orientations use an angular separation of 30^o between the incoming starlight of the guide and science interferometers; and the best-case orientations assume both interferometers are viewing the same star (*i.e.*, no separation, as above). Consistent with Table 2, four cases (A, B, C, and D) are assessed.

	Best-case Baselines	**Worst-case Baselines**
Best-case Orientations	Case A: s: (p2,n1) g: (p1,n2) no separation	Case B: s: (p1,n1) g: (p2,n3) no separation
Worst-case Orientations	Case C: s: (p2,n1) g: (p1,n2) 30^o separation	Case D: s: (p1,n1) g: (p2,n3) 30^o separation

Table 2: DWT Disturbance analysis cases used to evaluate the effectiveness of angle feedforward. For all cases no vibration isolation nor structural quieting is used.

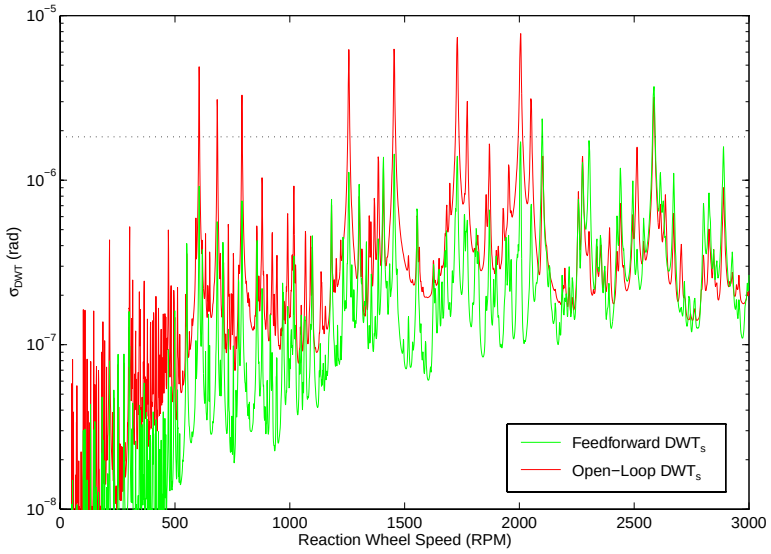

Figure 9: Angle feedforward effectiveness, Case A: science interferometer (p2,n1), guide interferometer (p1,n2), no angular separation between guide and science targets.

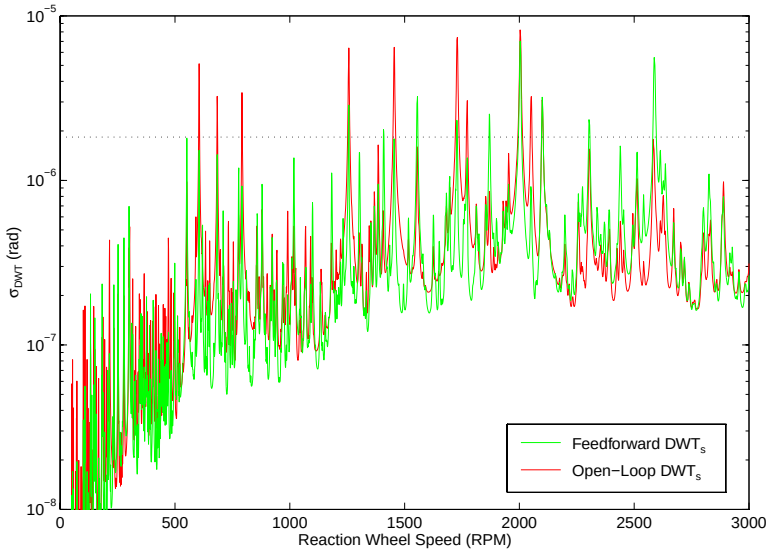

Figure 10: Angle feedforward effectiveness, Case B: science interferometer (p1,n1), guide interferometer (p2,n3), no angular separation between guide and science targets.

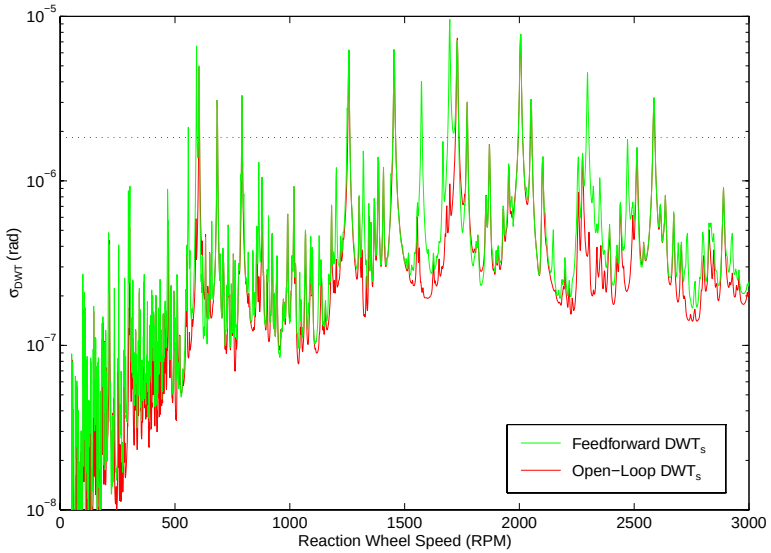

Figure 11: Angle feedforward effectiveness, Case C: science interferometer (p2,n1), guide interferometer (p1,n2), 30^o separation between guide and science targets.

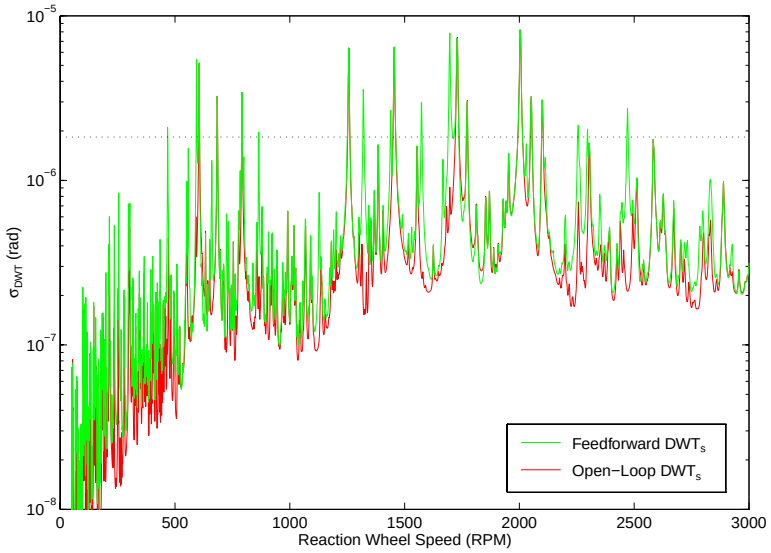

Figure 12: Angle feedforward effectiveness, Case D: science interferometer (p1,n1), guide interferometer (p2,n3), 30^o separation between guide and science targets.

The results of the disturbance analysis for these four cases are shown in Figures 9–12, with each plot displaying the total DWT with and without feedforward for a given case. When both interferometers are viewing the same star (cases A and B) the angle feedforward provides significant improvement. However, when the guide and science interferometers are viewing stars at the limit of expected angular separation (cases C and D), the angle feedforward results in no improvement whatsoever. In other words, the angle feedforward has limited effectiveness.

It has been suggested that a coordinate transformation could account for the effect of differing siderostat orientations. Unfortunately, the projection of the science siderostat motion onto the normal vector of the guide siderostat does not cause any guide wavefront tilt. This can be thought of as a null space in the sensitivity of the interferometer wavefront tilt to siderostat rotation, where the null space corresponds to rotation of the siderostat about the normal vector. Since the two sets of siderostats have different orientations, they also have different null spaces. Hence, a vector component of the motion that affects the wavefront tilt of the science interferometer is not observed by the guide interferometer. This vector component cannot be reconstructed with the transformation. The transformation could only account for the the science siderostat motion projected onto the tip/tilt axes of the guide interferometer. Roughly speaking, the unobservable residual motion would be of the same order as the residual without the use of the transformation.

If improved optical control were required for the science interferometer, some type of

sensors would have to be added. These potential sensors could be either inertial or optical. Inertial sensors would measure the orientations of the optical elements in inertial space, from which DWT could be inferred. Either gyroscopes or accelerometers could be used, but in both instances the gains of sensors on corresponding mirrors of the two interferometer arms would have to be matched. However, since wavefront tilt is most sensitive to siderostat motion (because of the beam compression just following the siderostat), it would most likely be sufficient to measure only the orientations of the siderostats. An optical metrology sensor would measure the wavefront tilt directly, much like the pathlength internal metrology. For example, this could be done by adding two internal metrology laser beams around the perimeter of the aperture, 90^o apart. The three internal metrology measurements would effectively provide piston (OPD) and tip/tilt (DWT in two axes).

Conclusion

An analysis has been described that was performed on the SIM integrated model version 1.0 in order to address the problem of meeting the total differential wavefront tilt requirement in the presence of mechanical disturbances. The disturbance analysis uses reaction wheels as the primary vibration source. The analysis uses a single RWA with the DWT requirement separated out for each wheel, effectively assuming that wheel orientation has negligible effect. This assumption is good to within a factor of three, *i.e.*, the worst-case RWA orientation yields a DWT a factor of three larger than the best-case orientation. Since the worst-case orientation is used, the analysis is conservative by less that a factor of two. Furthermore, a structural modal damping of 0.1% was assumed, consistent with values estimated on the MPI Testbed. However, there is evidence to suggest that modal damping may increase to 1% in a spaceborne environment. If this is the case, then the results are conservative by another factor of ten.

Even with the margin in the analysis, it was found that vibration isolation alone was sufficient to meet the DWT requirements. Specifically, a hexapod isolator with a pogo-mode break frequency of ≤ 4 Hz is necessary. This can be considered an isolation requirement. Furthermore, the analysis assumed an isolator modal damping of 10%, consistent with an actively-damped or viscous isolator. These results should be viewed with some caution, as isolation is effective only for targeted disturbances at discrete locations. Isolation would be ineffective for distributed disturbances such as structural creak or atmospheric buffeting. Even so, RWA disturbances are expected to be far and away the most significant. Furthermore, OPD has yet to be evaluated, although the derived isolator requirements are expected to be less stringent based on the results of previous interferometer disturbance analyses.

An analysis methodology was described for evaluating angle feedforward, which involves two interferometers, with a single-baseline, parameterized model. Although, angle

feedforward was not necessary to meet the DWT requirements, its effectiveness was investigated in the absence of isolation and structural quieting. With both interferometers viewing in the same direction, angle feedforward provides significant improvement regardless of the choice of baselines. However, when viewing stars separated by 30^o the angle feedforward yields no improvement, even when the most similar baselines are chosen. Overall the effectiveness of angle feedforward is limited. In order to be effective angle feedforward would have to add cumbersome instrument scheduling constraints in terms of baseline combinations and star separation limits.

Implications for SIM Instrument Design

On SIM, angle feedforward would be implemented by encoding the fast steering mirrors (FSMs) and the siderostat gimbals in the guide interferometer beam trains, and feeding that information forward to the science interferometer FSMs and gimbals. The science interferometer actuators would have local loops closed around their own encoders. All of these encoders need accuracies at the diffraction limit in order to accomplish this task. Since the angle feedforward is not needed, the angle sensor requirements are considerably relaxed. High resolution encoding is still necessary for those mounts which need feedback in order to maintain position during acquisition, but encoding accuracy need only meet the requirements of star acquisition [20].

References

[1] R.A. Laskin, M. San Martin, "Control/Structure System Design of a Spaceborne Optical Interferometer," Paper AAS–89–424, AAS/AIAA Astrodynamics Specialist Conference, Stow, Vermont, August, 1989.

[2] J.Spanos, *et al.*, "Control Structure Interaction in Long Baseline Interferometers," 12^{th} IFAC Symposium on Automatic Control in Aerospace, Ottobrun, Germany, September, 1992.

[3] M. Milman, *et al.*, "Integrated Modeling of Optical Systems User's Manual, Release 2.0," JPL D–13040, November 15, 1995.

[4] D. Redding, "Controlled Optics Modelling Package User Manual, Release 1.0," JPL D–9816, June 1, 1992.

[5] J. W. Melody, G. W. Neat, "Integrated Modeling Methodology Validation Using the Micro-Precision Interferometer Testbed", Proceedings of the 35^{th} IEEE Conference on Decision and Control, Kobe, Japan, December 1996.

[6] J.W.Melody, "SONATA Integrated Model and Open Loop Disturbance Analysis," JPL IOM 3411–95–235csi, June 26, 1995.

[7] J.W.Melody, "ISIS Integrated Model and RCS Thruster Disturbance Analysis," JPL IOM 3411–96–174ITP, May 20, 1996.

[8] J.W.Melody and H.C.Briggs, "Analysis of Structural and Optical Interactions of the Precision Optical Interferometer in Space (POINTS)," Proceedings of the SPIE Symposium on OE/Aerospace,

Science and Sensing, Conference on Spaceborne Interferometry, vol. 1947, pp. 44–57, Orlando, FL, April 1993.

[9] L.Jandura, personal communication, July, 1996.

[10] E.Schmidtlin, personal communication, July, 1996.

[11] E.F.Crawley, M.S.Barlow, M.C.von Schoor, B.P.Masters, A.S.Bicos, "Middeck Zero-Gravity Dynamics Experiment: Comparison of Ground and Flight Test Data," 43^{rd} Congress of International Astronomical Federation, Washington, D.C., September, 1992.

[12] "EURECA Micro-Gravity Measurement Subsystem: Post-flight Evaluation," ESA Final Report, December, 1994.

[13] M.H.Milman, C.-C.Chu, "Optimization Methods for Passive Damper Placement and Tuning," *AIAA Journal of Guidance, Control, and Dynamics*, Volume 17, Number 4, July-August, 1994, pp. 848–856.

[14] J.W.Melody, "Discrete-Frequency and Broadband Reaction Wheel Disturbance Models," JPL IOM 3411–95–200csi, June 1, 1995.

[15] G.W.Neat, J.W.Melody, "Hybrid Experimental/Analytical Method to Establish Technology Readiness for Spaceborne Interferometry," submitted to *IEEE Transactions on Control Systems Technology*, April, 1996.

[16] M.Colavita, "Visibility and Phasing," JPL IOM, August 10, 1994.

[17] J.M.Maciejowski, *Multivariable Feedback Design*, Addison-Wesley Publishing Company, Inc., New York, 1989.

[18] J.F.O'Brien, G.W.Neat, "Micro-Precision Interferometer: Pointing Control System," 4^{th} Conference on Control Applications, Albany, NY September, 1995.

[19] M.Milman, "Feedforward signal and guide star interferometer geometry," JPL IOM 3456–96–029, May, 1996.

[20] M.Colavita, personal communication, November, 1996.